Title: Bomb radiocarbon evidence for strong global carbon uptake and turnover in terrestrial vegetation

Authors: Heather D. Graven[1,*], Hamish Warren[1], Holly K. Gibbs[2], Samar Khatiwala[3], Charles Koven[4], Joanna Lester[1], Ingeborg Levin[5,†], Seth A. Spawn-Lee[6,7], and Will Wieder[8]

Affiliations:

[1]Department of Physics, Imperial College London, UK

[2]Nelson Institute for Environmental Studies and the Department of Geography, University of Wisconsin-Madison, USA

[3]Department of Earth Sciences, University of Oxford, UK

[4]Climate and Ecosystem Sciences Division, Lawrence Berkeley National Laboratory, USA

[5]Institute of Environmental Physics, Heidelberg University, Germany

[6]Department of Integrative Biology, University of Wisconsin-Madison, USA

[7]The Nature Conservancy, USA

[8]Climate & Global Dynamics, National Center for Atmospheric Research, and Institute of Arctic and Alpine Research, University of Colorado, USA

[*]Corresponding author. Email: h.graven@imperial.ac.uk

[†]Deceased

Abstract: Vegetation and soils are taking up approximately 30% of anthropogenic CO_2 emissions because of small imbalances in large gross carbon exchanges from productivity and turnover that are poorly constrained. We combine a new budget of radiocarbon (^{14}C) produced by nuclear bomb testing in the 1960s with model simulations to evaluate carbon cycling in terrestrial vegetation. We find that most state-of-the-art vegetation models used in the Coupled Model Intercomparison Project underestimate the ^{14}C accumulation in vegetation biomass. Our findings, combined with constraints on vegetation carbon stocks and productivity trends, imply that net primary productivity is likely at least 80 PgC/yr presently, compared to 43-76 PgC/yr predicted by current models. Storage of anthropogenic carbon in terrestrial vegetation is likely more short-lived and vulnerable than previously predicted.

One-Sentence Summary: Carbon uptake into vegetation is underestimated, but the carbon is turned over quickly.

Main Text:

The processes contributing to the net sink of CO_2 in the terrestrial biosphere are not yet well understood and will likely change in the future (*1*), making it difficult to predict future climate change and create effective mitigation and adaptation policies. Future climate predictions require robust representation of the global carbon cycle, which is challenging when basic properties still have large uncertainties. In particular, observational constraints on global net primary productivity (NPP) - the rate of creation of new plant tissues and products - and on carbon turnover rates are lacking. Estimates of global NPP rely on statistical or model-based estimates that use site-scale data (*2*); however, it is very difficult to measure all components of NPP (*3*) and there are not many sites with comprehensive measurements, especially in the tropics (*4*). A large range of global NPP of 43-76 PgC/yr is currently simulated by models (*5, 6*), and models do not generally show a strong trend over the 20th century, in conflict with the trend found for gross primary productivity (+30%) (*7*), which is typically twice as large as NPP. Here we provide global-scale constraints on NPP and carbon turnover by analyzing radiocarbon (^{14}C) produced by nuclear bomb testing and models of the terrestrial biosphere and vegetation.

Global bomb radiocarbon budget

Nuclear bomb testing in the 1950s and 1960s produced excess radiocarbon (^{14}C) in the atmosphere (Figure 1a), which was assimilated into the terrestrial biosphere and ocean through photosynthesis and air-sea gas exchange over time. Tracking how ^{14}C accumulated in the terrestrial biosphere after the bomb testing can therefore enable evaluation of the rates of carbon uptake and turnover (*8*). However, the global accumulation of ^{14}C in the biosphere cannot be observed directly: from new leaves to highly aged soil carbon, there is too much heterogeneity in ^{14}C content in the biosphere.

We use a budgeting approach to diagnose the ^{14}C accumulation in the terrestrial biosphere caused by bomb testing in order to evaluate carbon cycling in terrestrial biosphere models. In this approach, the ^{14}C accumulation in the terrestrial biosphere is calculated using observations in the stratosphere and troposphere and observationally-constrained ocean models to close the ^{14}C budget. In contrast to prior work (*9*) that examined the period 1945-2000, here we focus on the period 1963-67, when atmospheric ^{14}C was highly elevated relative to the biosphere but when no significant detonations took place (blue area in Figure 1a). Therefore, total ^{14}C in the Earth system was roughly constant but exchanged between reservoirs over 1963-67. This allows us to focus on the period where there is good observational coverage of the stratosphere by aircraft and balloon sampling, and to avoid uncertainty and assumptions with calculating the total ^{14}C produced by the bombs and estimating the pre-bomb ^{14}C content. Another advantage of focusing on 1963-67 is that we sharpen the constraint on ^{14}C uptake and turnover in vegetation, where the ^{14}C first entered the terrestrial biosphere, before much ^{14}C was transferred to litter and soil pools.

We use stratospheric data originally published in reports of the Health and Safety Laboratories, which were reassessed and recalculated with corrected standard values (*10-12*) and used in an atmospheric model to calculate global stratospheric ^{14}C inventories (*11*) (Figure 1). Tropospheric ^{14}C inventories were calculated from global compilations recently produced for modelling purposes (*13, 14*). Ocean ^{14}C simulations (*15-18*) that match revised ocean ^{14}C inventories (*19, 20*) from the 1970s (GEOSECS) and 1990s (WOCE) were used for ocean ^{14}C inventories.

After the ^{14}C was initially deposited in the stratosphere, the stratosphere lost roughly 200×10^{26} atoms of ^{14}C through mixing of the ^{14}C into the troposphere over 1963-67, which experienced a net gain of about 40×10^{26} atoms. The ocean gained about 80×10^{26} atoms through air-sea exchange (Figure 1b). We estimate that the terrestrial biosphere therefore must have accumulated $86\pm18 \times10^{26}$ atoms (95% confidence) [21] over 1963-67 (Figure 1c) as the assimilation of ^{14}C outpaced the turnover of ^{14}C back to the air.

Terrestrial biospheric ^{14}C accumulation in the CESM2 model

The terrestrial biospheric ^{14}C accumulation over 1963-67 provides a new constraint on coupled climate-carbon cycle models (also known as Earth system models or ESMs), which are used to inform global climate policy but have particularly uncertain terrestrial carbon cycle components due to the heterogeneity and complexity of land ecosystems. Simulations of the only such land model to simulate ^{14}C explicitly within an ESM, the Community Land Model version 5.0 (CLM5.0) [22], accumulate a much lower amount of ^{14}C in the terrestrial biosphere (about 40×10^{26} atoms) than our observation-based estimate ($86\pm18 \times10^{26}$ atoms, Figure 1c). Simulations of CLM5.0 driven with observed climate data (CLM5.0-unc, "uncoupled") [23] and coupled model simulations of the Community Earth System Model 2 [24] Large Ensemble Project (CESM2-LENS) [25][26] following the Coupled Model Intercomparison Project (CMIP) phase 6 historical (concentration-driven) simulation protocol show similar ^{14}C accumulation, and the spread across 9 ensemble members is small (Figure 1c). CLM5.0-unc results are similar to another offline simulation of CLM5.0 that suggested the ^{14}C accumulated in the terrestrial biosphere in the 1960s could be too small [27].

In 1963-67 not much bomb ^{14}C had yet entered the soil; most biospheric bomb ^{14}C was in vegetation (Figure 1c). In CESM2-LENS, 56% of the ^{14}C accumulated in vegetation, with only 18% in litter and coarse woody debris and 26% in soils over 1963-67. If the ^{14}C accumulation in vegetation in CESM2 were correct, then the ^{14}C accumulation in non-vegetation pools would have to be >3 times larger than simulated in CESM2-LENS and >75% of the total ^{14}C accumulation to match the observation-based estimate. It is unlikely that more than half of the biospheric ^{14}C accumulation over 1963-67 occurred in dead plant material and soils since the peak in global mean tropospheric ^{14}C occurred only in 1964-65.

We thus conclude that the ^{14}C accumulation in vegetation over 1963-67 in CESM2 is too low (Figure 1). The underestimate for vegetation could be because the NPP in the model is too low, so that not enough ^{14}C enters the vegetation, and/or because carbon is misallocated between short-lived vs long-lived pools, so that ^{14}C is turned over too quickly.

Vegetation model emulators and model-data comparisons

CESM2 is the only Earth system model with explicit simulations of ^{14}C available. Therefore, to simulate the ^{14}C accumulation in other models as well as to explore the sensitivity of the ^{14}C accumulation to NPP and carbon stocks, we need to construct emulator models. We found that the variables included in CMIP were not sufficient to construct a reliable emulator model for the whole terrestrial biosphere for CESM2, but that ^{14}C in vegetation could be modeled reliably (Figures 2-4).

We focus now on analyzing the ^{14}C accumulation only in vegetation in models over 1963-67. We constructed a simple emulator model for woody (long-lived: stem and coarse roots) and non-woody vegetation biomass (short-lived: leaves, fine roots and other pools), run on each model grid cell (21). We applied the emulator model to CESM2-LENS member 1001.001 and to models from CMIP5 and CMIP6 that reported the necessary variables. We examine global sums for woody and non-woody pools across all biomes and grid cells (Figures 2-4 and S1), so that global non-woody vegetation biomass includes the non-woody vegetation biomass in forests as well as other biomes. We compare with satellite-based vegetation carbon products (29-31) that omit leaf carbon in forests, so we estimated global total leaf carbon in forests to be 14.3 PgC (based on Table S5 in reference (32)) and added this to the observation-based estimates of vegetation carbon stocks.

To evaluate the vegetation ^{14}C simulations, we estimate the true ^{14}C accumulation in vegetation by subtracting the ^{14}C accumulation in litter, coarse woody debris and soils simulated by CESM2-LENS member 1001.001 from the observation-based total terrestrial biosphere ^{14}C accumulation over 1963-67. We allow the uncertainty in non-vegetation ^{14}C accumulation to be ±100% (95% confidence) (21), even though CESM2/CLM5 is in fact likely to overestimate this ^{14}C accumulation since its proportion of fresh carbon in both surface and sub-surface soils has been shown to be too high (33). Our estimate of vegetation ^{14}C accumulation is $69\pm24 \times10^{26}$ atoms (95% confidence) over 1963-67 at 95% confidence, which allows for a possible range of 43-100% of biospheric ^{14}C accumulation in vegetation.

Most of the CMIP5 and CMIP6 vegetation emulator models underestimate the observation-based vegetation ^{14}C accumulation over 1963-67 (5 of 7 models, Figure 2). The two models that match the observation-based vegetation ^{14}C accumulation have high NPP of more than 68 PgC/yr in 1965 (Figure 2b, Figure S1, Table S1). One of the two models is from CMIP5 (IPSL5), whereas the CMIP6 version of that model (IPSL6) has much lower NPP and underestimates the observation-based vegetation bomb ^{14}C inventory. The other model matching the observation-based vegetation bomb ^{14}C inventory, CanESM5 from CMIP6, has high NPP and allocates a large fraction of its NPP to wood (68% in 1965), in contrast to other models that allocate 22-43% of NPP to wood (Table S1).

Overall, the ^{14}C accumulation in vegetation over 1963-67 shows a strong relationship with NPP but not with vegetation carbon stock (Figure 2). This indicates that higher NPP increases ^{14}C accumulation in vegetation over 1963-67 but higher carbon stock (and slower turnover rate) generally does not. Two versions of the MRI model lie below a regression line between ^{14}C accumulation in vegetation and NPP for the other five models (Figure 2b). The MRI models allocate the highest fraction of NPP to non-woody vegetation (76-78% to non-woody, 22-24% to woody) and their non-woody annual NPP is similar to their non-woody carbon stock (Table S1), which indicates a very high level of productivity per unit biomass and fast turnover rate. Therefore, the flux of ^{14}C into non-woody vegetation in the MRI models is large but it is turned over quickly and the ^{14}C accumulation in non-woody vegetation is among the lowest (Figure 3a).

There are differing controls on ^{14}C accumulation over 1963-67 in non-woody vs woody vegetation biomass in the emulator models (Figures 3, S2 and S3). Accumulation of ^{14}C in longer-lived woody vegetation is sensitive to NPP, while accumulation of ^{14}C in shorter-lived non-woody vegetation is more sensitive to the carbon stock. At higher stocks of non-woody vegetation carbon, ^{14}C accumulation in non-woody vegetation is also sensitive to NPP. The

patterns found for scaling experiments in the CESM2 vegetation emulator (contours in Figure 3) are similar to the patterns found for the other vegetation model emulators (colored symbols in Figure 3).

The patterns in Figure 3 indicate that underestimated ^{14}C accumulation in vegetation over 1963-67 is due to underestimated NPP or underestimated non-woody vegetation biomass in models. Only IPSL6 underestimates the total vegetation carbon stock estimated with satellite data (Figure 2c, Figure S4), so increasing non-woody carbon stock in the models requires that carbon shifts from woody biomass (stems and coarse roots) to non-woody biomass (leaves, fine roots and other biomass) by adjustment of their turnover rates. The models tend to underestimate belowground vegetation carbon stocks (*29, 30*) (Figure S5), so shifting aboveground woody carbon (stems) to belowground non-woody carbon (fine roots) in particular may be required. On the other hand, NPP in woody (or non-woody) vegetation could be increased in the models without necessarily affecting carbon stocks, if modelled turnover rates are simultaneously increased.

The regression between vegetation ^{14}C accumulation and NPP (R^2>0.99), excluding the MRI models that have very high non-woody NPP, suggests that NPP in 1965 should have been at least 63 PgC/yr (the value of NPP at the intersection of the regression line and ^{14}C accumulation uncertainty range in Figure 2b). However, only 16% of all CMIP6 models have NPP higher than 63 PgC/yr in 1965 (Figure 2d, Table S2). Considering that total carbon assimilation (Gross Primary Productivity or GPP) increased by ~30% over the 20th century (*7*), if carbon uptake efficiency (NPP/GPP) did not change significantly then NPP should be at least 80 PgC/yr presently, while it is only 43-76 PgC/yr in current models (*5*).

Implications for the carbon cycle

The simulations of ^{14}C we analysed provide evidence that CESM2 and most other CMIP6 models underestimate the magnitude of NPP in the 1960s. The minimum NPP of 63 PgC/yr in 1965 and 80 PgC/yr recently (applying a 30% increase following (*7*)) that is implied by our analysis of bomb ^{14}C in vegetation is higher than simulated in most CMIP6 models (*5*) (Figure 2) but within the higher end of the range of observation-based estimates of GPP (*34-37*), assuming roughly 50% NPP/GPP. The global NPP/GPP ratio might increase slightly in the future (*38*), but we are not aware of any evidence for a historical trend. The average NPP in CMIP6 models actually decreased in comparison with CMIP5 models (*5, 39*), which likely degraded the model cohort rather than improved it.

Our results highlight parametric and structural uncertainties in model simulations of leaf-level photosynthesis and stomatal conductance, nutrient limitation, autotrophic respiration, carbon allocation, mortality and turnover. For example, replacing the widely-used assumption of homogeneity in wood carbon turnover rates at a given location (*40*) with vegetation demographic models (*41*) that allow distinct populations of fast-growing versus long-lived trees may improve ^{14}C accumulation, where the former are able to rapidly take up ^{14}C while the latter dominate the overall biomass pool (*42*). However, since ^{14}C accumulation over 1963-67 is higher in woody than non-woody vegetation (Figures 3, S1 and S4), it is likely that increasing NPP to woody vegetation in models that underestimate ^{14}C accumulation is required. Satisfying observational constraints on carbon stocks while increasing NPP will require that the rate of carbon turnover in the models also increases.

A range of 41-64 PgC/yr for NPP was found in a previous study (9) using a ^{14}C budget to diagnose the bomb-produced ^{14}C in the biosphere, and then using this budget to fit parameters in a simple 3-box global biosphere model (43). Our evaluation of state-of-the-art global biosphere models suggests that the ^{14}C budget in the 1960s cannot be met with NPP lower than 63 PgC/yr in current model formulations (Figure 2b). This is in fact consistent with reference (9) whose budget was not closed in the 1960s and instead included a residual "hidden sink", which must be in the terrestrial biosphere.

Radiocarbon data provide powerful and unique insights on carbon cycling and model evaluation, but they have been underutilized due to the low number of models simulating [14]C. In addition to the observation-based global ^{14}C accumulation used here and soil carbon ^{14}C data used previously to evaluate CMIP models (33, 44), other data including ^{14}C in specific soil compounds, in respiration or in atmospheric CO_2 could be used to evaluate more processes in models that simulate [14]C. Analyzing the 1963-67 period allowed us to focus on vegetation, but longer analysis of subsequent decades would enable critical insights on whole ecosystem cycling including litter and soil (Figure 1c). Within vegetation alone, ^{14}C simulations strongly diverge over time (Figure 2a) and there are large differences between models in their spatial distribution of ^{14}C accumulation, NPP and carbon stock (Figure 4 and S6). Spatial differences in ^{14}C accumulation between models are at least a factor of two but up to a factor of 10 for non-woody vegetation in northern temperate and boreal regions. Additional ^{14}C data-model comparison will enable more constraints on various processes. Also, since we estimated the 1963-67 ^{14}C accumulation in litter and soils based on the CESM-LENS simulations (with ±100% uncertainty), further analysis of ^{14}C through all biospheric pools would help to refine the constraints on vegetation.

The vegetation emulator model we used represents the ^{14}C explicitly simulated in CESM2 well (Figures 2-4), but the emulator could not be evaluated for other models and emulators for litter and soil pools could not be constructed with the limited variables in the CMIP output. Ensuring an accurate representation of ^{14}C in biospheric models requires that the models explicitly simulate ^{14}C, which only requires one additional tracer to be added in a simple way (21). New methods for fast spin up could be exploited (45-47). As requested for CMIP6 (48), we strongly recommend that modelling groups implement ^{14}C in ESMs and in stand-alone models, and report these results to CMIP and related activities to enable model assessment and scientific understanding.

Accurate simulation of vegetation and total biospheric carbon uptake and turnover is critical to understanding historical and future anthropogenic carbon storage in terrestrial ecosystems, both for natural sinks of CO_2 as well as for 'nature-based solutions' that aim to remove atmospheric CO_2 by increasing land ecosystem carbon. Our analysis shows that the uptake of carbon via NPP and the rate of carbon turnover in models must both be increased, which will increase the turnover of anthropogenic carbon in the terrestrial biosphere. Since the uptake and turnover of carbon are the main controls on the anthropogenic CO_2 sink in the terrestrial biosphere, this study shows that the storage of anthropogenic carbon in the terrestrial biosphere is likely more short-lived and more vulnerable to future changes than previously thought.

References and Notes

1. P. Friedlingstein *et al.*, Global Carbon Budget 2023. *Earth Syst. Sci. Data* **15**, 5301-5369 (2023).

2. A. Ito, A historical meta-analysis of global terrestrial net primary productivity: are estimates converging? *Global Change Biology* **17**, 3161-3175 (2011).

3. D. A. Clark *et al.*, Measuring Net Primary Production in Forests: Concepts and Field Methods. *Ecological Applications* **11**, 356-370 (2001).

4. R. J. Olson, J.M.O. Scurlock, S.D. Prince, D.L. Zheng, and K.R. Johnson*, O. R. N. L. D. A. A. Center, Ed. (Oak Ridge, Tennessee, USA, 2013).

5. R. M. Varney, S. E. Chadburn, E. J. Burke, P. M. Cox, Evaluation of soil carbon simulation in CMIP6 Earth system models. *Biogeosciences* **19**, 4671-4704 (2022).

6. M. Zhao, F. A. Heinsch, R. R. Nemani, S. W. Running, Improvements of the MODIS terrestrial gross and net primary production global data set. *Remote Sensing of Environment* **95**, 164-176 (2005).

7. J. E. Campbell *et al.*, Large historical growth in global terrestrial gross primary production. *Nature* **544**, 84-87 (2017).

8. S. E. Trumbore, Age of Soil Organic Matter and Soil Respiration: Radiocarbon Constraints on Belowground C Dynamics. *Ecological Applications* **10**, 399-411 (2000).

9. T. Naegler, I. Levin, Observation-based global biospheric excess radiocarbon inventory 1963–2005. *Journal of Geophysical Research* **114**, D17302 (2009).

10. T. Naegler, Simulating bomb radiocarbon: Consequences for the global carbon cycle, PhD Thesis, Univ. of Heidelberg, Heidelberg, Germany (2005).

11. T. Naegler, I. Levin, Closing the global radiocarbon budget 1945–2005. *J Geophys Res* **111**, D12311 (2006).

12. V. Hesshaimer, I. Levin, Revision of the stratospheric bomb $^{14}CO_2$ inventory. *J Geophys Res* **105**, 11641-11658 (2000).

13. H. Graven *et al.*, Compiled records of carbon isotopes in atmospheric CO_2 for historical simulations in CMIP6. *Geosci. Model Dev.* **10**, 4405-4417 (2017).

14. M. Meinshausen *et al.*, Historical greenhouse gas concentrations for climate modelling (CMIP6). *Geosci Model Dev* **10**, 2057-2116 (2017).

15. H. D. Graven, N. Gruber, R. Key, S. Khatiwala, X. Giraud, Changing controls on oceanic radiocarbon: New insights on shallow-to-deep ocean exchange and anthropogenic CO_2 uptake. *J Geophys Res* **117**, C10005 (2012).

16. S. Khatiwala, H. Graven, S. Payne, P. Heimbach, Changes to the Air-Sea Flux and Distribution of Radiocarbon in the Ocean Over the 21st Century. *Geophysical Research Letters* **45**, 5617-5626 (2018).

17. B. Pookkandy, H. Graven, A. Martin, Contemporary oceanic radiocarbon response to ocean circulation changes. *Climate Dynamics*, (2023).

18. J. G. Lester, "Changes in oceanic radiocarbon and CFCs since the 1990s. doi: 10.5281/zenodo.8242144," (Zenodo, 2023).

19. T. Naegler, Reconciliation of excess ^{14}C-constrained global CO_2 piston velocity estimates. *Tellus B* **61**, 372-384 (2009).

20. S. Peacock, Debate over the ocean bomb radiocarbon sink: Closing the gap. *Global Biogeochemical Cycles* **18**, (2004).

21. Materials and methods are available as supplementary materials online.

22. D. M. Lawrence *et al.*, The Community Land Model Version 5: Description of New Features, Benchmarking, and Impact of Forcing Uncertainty. *Journal of Advances in Modeling Earth Systems* **11**, 4245-4287 (2019).

23. CLM5.0 data are archived and publicly available at the UCAR/NCAR Climate Data Gateway (https://doi.org/10.5065/d6154fwh).

24. G. Danabasoglu *et al.*, The Community Earth System Model Version 2 (CESM2). *Journal of Advances in Modeling Earth Systems* **12**, e2019MS001916 (2020).

25. K. B. Rodgers *et al.*, Ubiquity of human-induced changes in climate variability. *Earth Syst. Dynam.* **12**, 1393-1411 (2021).

26. CESM2-LENS data are available at https://www.cesm.ucar.edu/community-projects/lens2

27. T. Frischknecht, A. Ekici, F. Joos, Radiocarbon in the Land and Ocean Components of the Community Earth System Model. *Global Biogeochemical Cycles* **36**, e2021GB007042 (2022).

28. UN, "United Nations Scientific Committee on the Effects of Atomic Radiation. Sources and Effects of Ionizing Radiation – Volume 1: Sources. UNSCEAR 2000 Report to the General Assembly, with Scientific Annexes. ISBN: 92-1-142238-8.," (United Nations, New York, 2000).

29. H. K. Gibbs, A. Ruesch, "New IPCC Tier-1 Global Biomass Carbon Map for the Year 2000. CDIAC, ESS-DIVE repository. Dataset. doi:10.15485/1463800," (2008).

30. S. A. Spawn, C. C. Sullivan, T. J. Lark, H. K. Gibbs, Harmonized global maps of above and belowground biomass carbon density in the year 2010. *Scientific Data* **7**, 112 (2020).

31. K.-H. Erb *et al.*, Unexpectedly large impact of forest management and grazing on global vegetation biomass. *Nature* **553**, 73-76 (2018).

32. P. B. Reich *et al.*, Temperature drives global patterns in forest biomass distribution in leaves, stems, and roots. *Proceedings of the National Academy of Sciences* **111**, 13721-13726 (2014).

33. Z. Shi *et al.*, The age distribution of global soil carbon inferred from radiocarbon measurements. *Nature Geoscience* **13**, 555-559 (2020).

34. C. Beer *et al.*, Terrestrial gross carbon dioxide uptake: global distribution and covariation with climate. *Science* **329**, 834-838 (2010).

35. L. R. Welp *et al.*, Interannual variability in the oxygen isotopes of atmospheric CO2 driven by El Nino. *Nature* **477**, 579-582 (2011).

36. G. Badgley, L. D. L. Anderegg, J. A. Berry, C. B. Field, Terrestrial gross primary production: Using NIRV to scale from site to globe. *Global Change Biology* **25**, 3731-3740 (2019).

37. M.-C. Liang *et al.*, New constraints of terrestrial and oceanic global gross primary productions from the triple oxygen isotopic composition of atmospheric CO2 and O2. *Scientific Reports* **13**, 2162 (2023).

38. J. M. Mathias, A. T. Trugman, Climate change impacts plant carbon balance, increasing mean future carbon use efficiency but decreasing total forest extent at dry range edges. *Ecol Lett* **25**, 498-508 (2022).

39. N. Wei *et al.*, Evolution of Uncertainty in Terrestrial Carbon Storage in Earth System Models from CMIP5 to CMIP6. *Journal of Climate* **35**, 5483-5499 (2022).

40. A. Wolf *et al.*, Forest biomass allometry in global land surface models. *Global Biogeochemical Cycles* **25**, (2011).

41. R. A. Fisher *et al.*, Vegetation demographics in Earth System Models: A review of progress and priorities. *Global Change Biology* **24**, 35-54 (2018).

42. J. A. Lutz *et al.*, Global importance of large-diameter trees. *Global Ecology and Biogeography* **27**, 849-864 (2018).

43. T. Naegler, I. Levin, Biosphere-atmosphere gross carbon exchange flux and the $\delta^{13}CO_2$ and $\Delta^{14}CO_2$ disequilibria constrained by the biospheric excess radiocarbon inventory. *J Geophys Res* **114**, D17303 (2009).

44. Y. He *et al.*, Radiocarbon constraints imply reduced carbon uptake by soils during the 21st century. *Science* **353**, 1419-1424 (2016).

45. Y. Luo *et al.*, Matrix Approach to Land Carbon Cycle Modeling. *Journal of Advances in Modeling Earth Systems* **14**, e2022MS003008 (2022).

46. H. Metzler *et al.*, Mathematical Reconstruction of Land Carbon Models From Their Numerical Output: Computing Soil Radiocarbon From C Dynamics. *Journal of Advances in Modeling Earth Systems* **12**, e2019MS001776 (2020).

47. S. Khatiwala, Fast Spin-Up of Geochemical Tracers in Ocean Circulation and Climate Models. *Journal of Advances in Modeling Earth Systems* **15**, e2022MS003447 (2023).

48. C. D. Jones *et al.*, C4MIP – The Coupled Climate–Carbon Cycle Model Intercomparison Project: experimental protocol for CMIP6. *Geosci Model Dev* **9**, 2853-2880 (2016).

49. CMIP5 and CMIP6 data available at: https://esgf-node.llnl.gov/projects/esgf-llnl/

Author contributions:

Conceptualization: HDG

Methodology: HDG, HW, CK, WW

Investigation: HDG, HW, HKG, SK, CK, JL, IL, SS, WW

Visualization: HDG, JL

Writing – original draft: HDG

Writing – review & editing: HDG, HW, HKG, SK, CK, JL, IL, SS, WW

Competing interests: Authors declare that they have no competing interests.
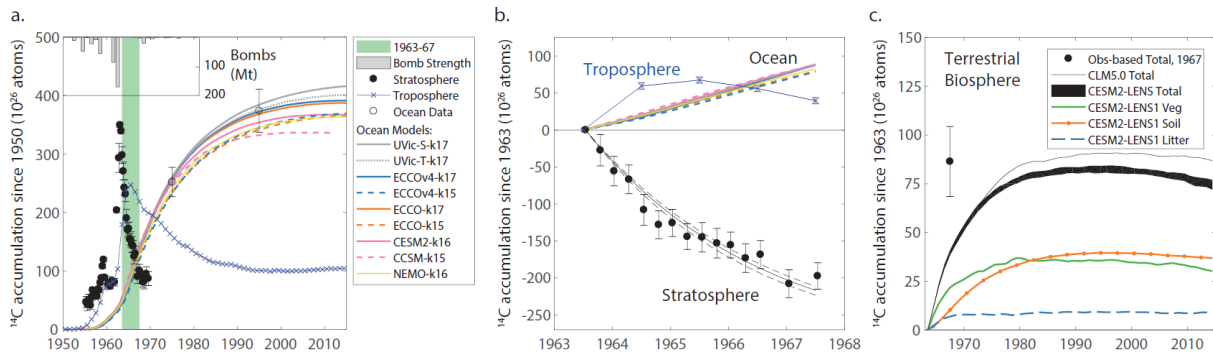
Supplementary Materials

Materials and Methods

Figs. S1 to S6

Tables S1 to S2

Data S1

Fig. 1. Budget of excess ^{14}C from nuclear bomb testing. (a) Accumulation of ^{14}C in the stratosphere (*11*), troposphere (*13, 14*) and ocean since 1950 based on observations, and simulated accumulation of ^{14}C in ocean models (*15-17*) selected to match observations (*19, 20*) in the 1970s and 1990s. Inset shows annual nuclear bomb strength in units of Mt TNT equivalent (*28*). The period 1963-67 with no significant bombs is highlighted in green. (b) ^{14}C accumulation in the stratosphere, troposphere and ocean since 1963, focusing on the period 1963-67 with no significant nuclear detonations (green area in a.). The black solid line shows an exponential fit to the stratospheric data and the dashed lines show the 1-σ uncertainty in the χ^2 fit. (c) Our new observation-based estimate of ^{14}C accumulation in the terrestrial biosphere in 1967 relative to 1963 (black circle), based on the budgeting approach, and simulations of the CLM5.0 model driven with observed climate data (CLM5.0-unc) or as part of the CESM2 model in the Large Ensemble (CESM2-LENS). The black area shows the range of ^{14}C accumulation in the terrestrial biosphere across 9 ensemble members. [14]C accumulation in vegetation, soils and litter (including coarse woody debris) are shown for CESM2-LENS ensemble member 1001.001.
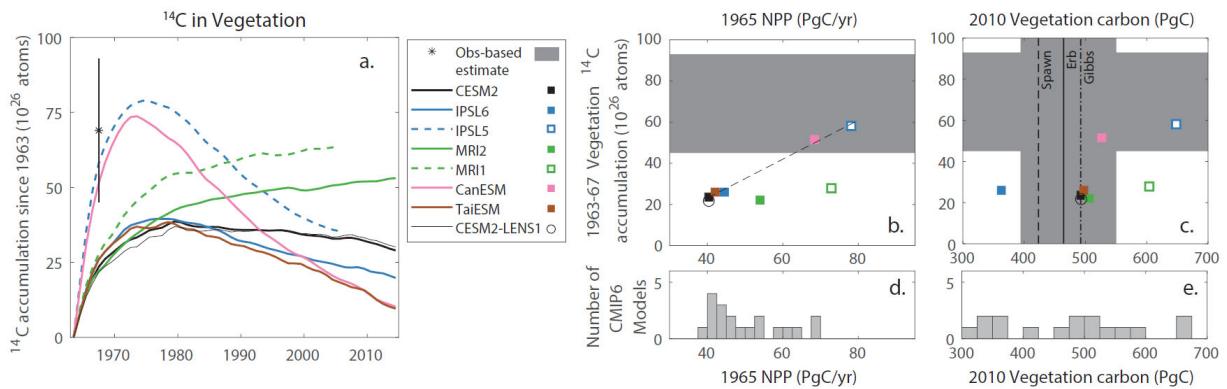
Figure 2. Model-data comparison for vegetation in the emulator models and in CESM2. (a) Simulated accumulation of ^{14}C in vegetation since 1963 compared with the observation-based estimate of ^{14}C accumulation in vegetation over 1963-67. (b) Accumulation of ^{14}C in vegetation over 1963-67 vs NPP in 1965 in each emulator model and CESM2, including a regression line for emulator models excluding MRI models. Gray area shows the uncertainty range in the observation-based estimate of ^{14}C accumulation. (c) Accumulation of ^{14}C in vegetation over 1963-67 vs carbon stock in vegetation in 2010 (2005 for MRI1 and IPSL5) in each emulator model and CESM2, including observation-based estimates of vegetation carbon stock (*29-31*) where the gray area reflects the uncertainty from Erb et al. (*31*) and uncertainty in ^{14}C accumulation. (d) and (e) show histograms of NPP in 1965 and carbon stock in vegetation in 2010 in CMIP6 models, including additional models that could not be included in the vegetation emulator simulations because the available CMIP6 output for these models lacked the necessary variables to run the emulator model (Table S2). The explicit simulation of ^{14}C in vegetation in CESM2-LENS member 1001.001 (CESM2-LENS1) is shown in (a-c) for comparison with the CESM2 vegetation emulator model.
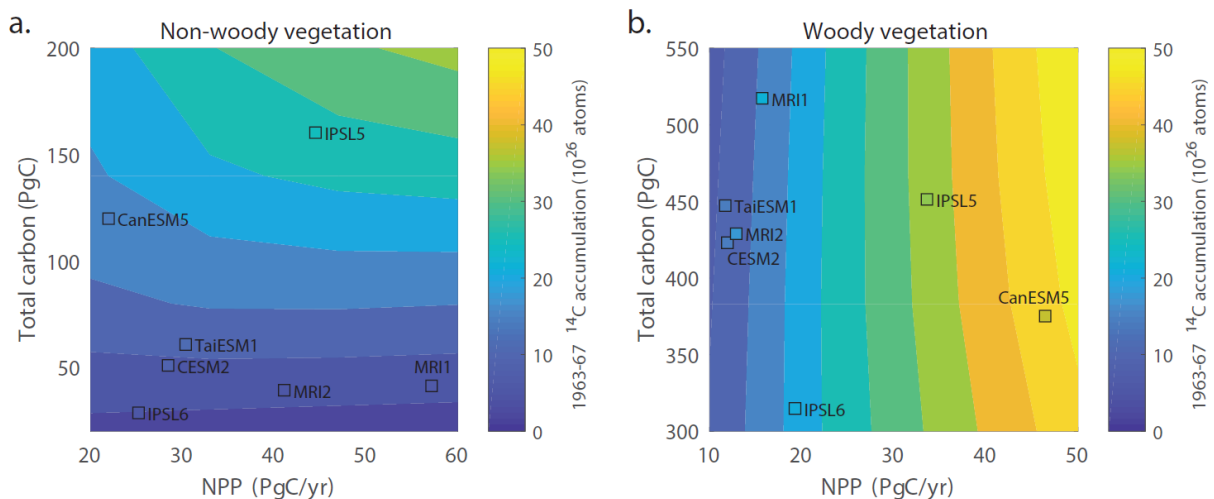
Figure 3. Sensitivity of ^{14}C accumulation to NPP and total carbon. Accumulation of ^{14}C over 1963-67 in non-woody (a) and woody (b) vegetation biomass plotted in color with NPP and total carbon stock in 1965 on x and y axes. Contours reflect relationships across 16 simulations of the CESM2 emulator where NPP and total carbon stock were scaled across the range shown here. Symbols show ^{14}C accumulation in the emulator models using the same color bar.
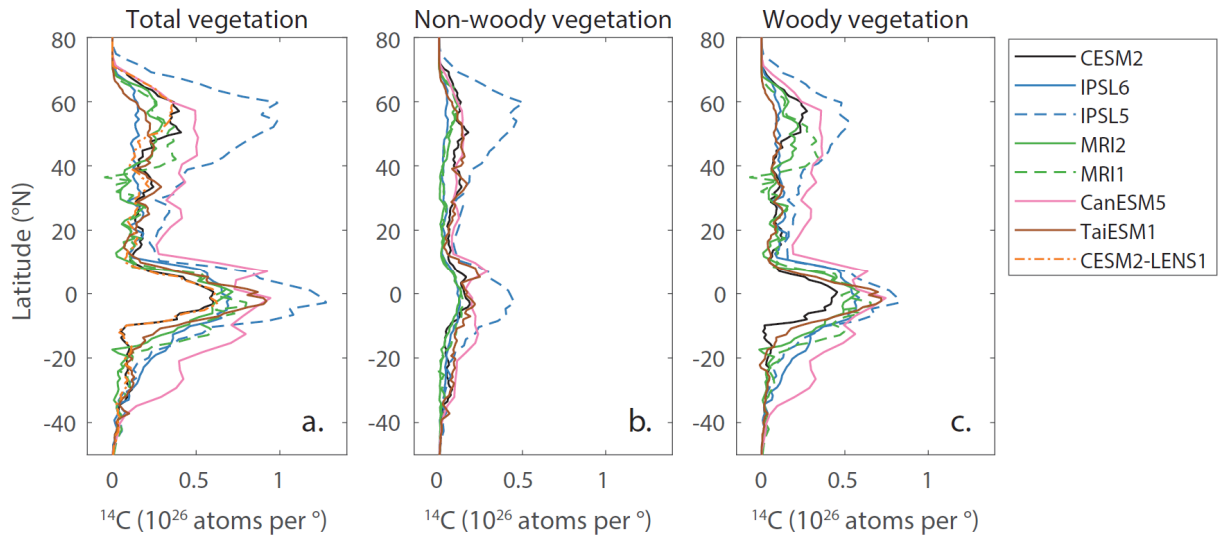
Fig. 4. Spatial distribution of ^{14}C accumulation simulated in vegetation in the emulator models and in CESM2. Accumulation of ^{14}C over 1963-67 per degree latitude in total (a), non-woody (b) and woody (c) vegetation biomass integrated over all longitudes. The explicit simulation of ^{14}C in CESM2-LENS1 is shown in (a) for comparison with the CESM2 emulator model.